Rotor Component Load Reconstruction for Fiber Bragg-Instrumented Rotor Blades

Tobias Pflumm
Technology & Innovation
Kopter Germany GmbH
Höhenkirchen-Siegertsbrunn, Germany

Dominik Komp
Technology & Innovation
Kopter Germany GmbH
Höhenkirchen-Siegertsbrunn, Germany

Benedikt Sosa
Chair of Rotorcraft and Vertical Flight
Technical University of Munich
Garching, Germany

Zeynep Bilgin
Chair of Rotorcraft and Vertical Flight
Technical University of Munich
Garching, Germany

Andreas Jochum
Technology & Innovation
Kopter Germany GmbH
Höhenkirchen-Siegertsbrunn, Germany

Sören Süße
Technology & Innovation
Kopter Germany GmbH
Höhenkirchen-Siegertsbrunn, Germany

ABSTRACT

Monitoring the loads on key rotor components during operation can help to reduce maintenance expenses and life cycle costs for helicopter operators. As such loads are typically challenging to measure, this study proposes a methodology for predicting loads on such components – including the pitch-link, the inter-blade damper and the rotor mast bending moment – based on the data obtained from a fiber Bragg-instrumented pre-series AW09 rotor blade. A full-scale whirl-tower rotor test campaign was conducted to investigate the relationship between instrumented rotor components and strain signals. Time-domain signals were converted to frequency-domain features, which were used to train a supervised regression model predicting the Fourier coefficients of the target load sensor based on the instrumented blade data. A linear regression analysis was conducted to assess the influence of specific blade instrumentation characteristics, including local deformation and sensor radial position, on model performance. Additionally, the performance of a neural network model was compared to that of the linear regression. It was demonstrated that an instrumented blade can be an effective means of estimating the loads on other rotor components. The accuracy of this approach was found to be significantly superior to that obtained by using only the control input data for the regression. The regression exhibited an improvement in accuracy as the number of sensors increased. While neural networks showed potential to capture complex, non-linear relationships in the data, a simpler linear regression model was sufficient to reconstruct the main characteristics of the target signal.

NOTATION

ANN	Artificial neural network
AREA	Autonoumous Rotorcraft for Extreme Altitudes
AW09	Kopter AW09 (single-engine helicopter)
AW139	Leonardo AW139 (twin-engine helicopter)
DIC	Digital image correlation
DFOSS	Direct fiber-optic shape sensing
EMC	Electromagnetic compatibility
FBG	Fiber Bragg grating
FFT	Fast Fourier transform
H135	Airbus Helicopters H135 (twin-engine helicopter)
HUMS	Health and usage monitoring system
HL	Hidden layer
iRoB	Instrumented rotor blade (BayLu25 project)
MERIT	Munich Experimental Rotor Investigation Testbed
S-N	Stress-life curve
TUM	Technical University of Munich
c_{12}	Linear shear strain / twist rate coefficient
F	Cross-sectional stress resultant vector
F_{pl}	Pitch-link force
F_D	Aft inter-blade damper force
K	Cross-sectional stiffness matrix
k	Linear gauge factor
M_y	Rotor-mast bending moment
N_C	Number of cycles
N_F	Number of terms in the Fourier series
N_R	Number of samples per revolution
N_S	Number of samples in dataset

Presented at the 50th European Rotorcraft Forum, Marseille, France, Sept. 10–12, 2024.

R^2	Coefficient of determination
T	Temperature
x, y, z	Spatial coordinates
α	Learning rate
ε	Strain tensor
ε_c	Cross-sectional strain vector
$\bar{\varepsilon}_1$	Axial strain
ζ	Thermo-optical coefficient
θ	Rotor controls
Ω	Rotational speed
κ_1	Twist rate
κ_2	Flap bending curvature
κ_3	Lead lag-bending curvature
$(.)_{mech}$	mechanical
$(.)_{therm}$	thermal

INTRODUCTION

Traditionally, helicopter component lifespans are estimated based on loads which are encountered during design and qualification, with adjustments for known fleet issues. However, actual in-flight loads are rarely measured on production aircraft, leaving these predictions conservative and vulnerable to unforeseen circumstances. It has been accepted that load monitoring on production aircraft has the potential to improve safety and to reduce maintenance costs. The adoption of this technology has been hindered by the limitations of traditional sensors and data acquisition systems, which are often bulky, heavy and unreliable in long-term use (Ref. 1).

Beyond that, EASA and national aviation authorities (Ref. 2) highlighted the need to expand health and usage monitoring systems (HUMS) to helicopter rotor components. While past research primarily focused on utilizing sensor data from the non-rotating reference frame, it became evident that fusing existing vibration measurements from the gearbox and the airframe with data collected from the rotating frame could significantly improve the detection of rotor system damage. Particularly noteworthy are the works of Chopra's research group (Refs. 3–8) at the University of Maryland and of MJA Dynamics by Azzam and Andrew (Refs. 9, 10).

It is desired to keep the investment and system costs as low as possible and to determine the load spectra of critical and maintenance-intensive components on the rotor. In recent years, notable research initiatives of Sikorsky (Ref. 1), Airbus Helicopters (Refs. 11, 12) and Leonardo Helicopters (Refs. 13, 14) demonstrated the establishment of a causal relationship between flight parameters and load condition with the use of neural networks. In these references, the Fourier coefficients of the high frequency dynamic time signal of the load variables were predicted based on quasi-stationary flight parameters such as aircraft altitude, airspeed, acceleration, attitudes, attitude rates, rotor speed and controls. The models were trained and evaluated on test and certification flight data of instrumented aircraft. The published studies and methods primarily used simple "Feed Forward Neural Networks", but also "Recurrent Neural Networks" and "Long-Short Term Memory" architectures.

In comparison, the research hypothesis of the current study and the *iRoB* (instrumented Rotor Blade) research project included an instrumentation of the rotor blade as it represents the ideal data source for load reconstruction and usage monitoring. This is due to the fact that the blade is mostly the origin of the aeromechanical loads on the helicopter rotor, which are transferred to other – possibly more maintenance-intensive and critical – rotor components. The composite structure of the rotor blades furthermore offers the opportunity to directly embed fiber-optic sensors in the form of fiber Bragg gratings (FBGs). This promises high robustness against weather, EMC protection and good fatigue properties. Furthermore, given the typically long life of rotor blades, they are ideal candidates for instrumentation, avoiding the need for frequent replacement.

Relevant references, which also explored the usage of FBGs on helicopter rotor blades in recent years, are summarized below. Hajek, Manner and Süße (Refs. 15, 16) from the Technical University of Munich (TUM) investigated the integration of FBG sensors into of a highly elastic blade root structure of a bearingless H135 rotor. The sensors were subsequently tested on a test bench and compared to strain gauges applied to the same structure. The authors concluded that the signal quality of the FBG sensors in terms of scatter, noise and linearity showed potential for future HUMS applications. Based upon the previous work, Süße and Hajek (Ref. 17) refined a method to analyze FBG strain measurements along the blade to not only determine its elastic deformation but also recover the bending stiffness coefficients at 15 different cross-sections of the AREA rotor blade (Ref. 18).

Bottasso et. al. (Ref. 19) described the development of a blade strain monitoring system for the tail rotor of the Leonardo AW139 helicopter. The system demonstrated the feasibility of a rotor-based interrogation system, as well as the embedding of FBG sensors into composite rotor blades. Key features of the study included the careful optimization of the fiber path considering blade manufacturing constraints, a temperature compensation method to decouple thermal strain, and an integrated interrogation-communication system. This self-contained unit, housed in a dedicated beanie, could withstand the harsh rotor hub environment and avoided the need for slip rings.

Particular noteworthy is also the project BladeSense, conducted by a consortium of Airbus Helicopters UK, Cranfield University, Helitune and BHR Group (Refs. 20–24), which utilized both FBGs for strain measurements and a direct fiber-optic shape sensing (DFOSS) approach based on differential interferometry for the recovery of deformation and the dynamic characterization of an H135 rotor blade. Beyond laboratory and test bench trials, the feasibility of the technology was evaluated through ground runs.

As part of the joint research project *iRoB* by Kopter Germany and TUM, Berghammer et al. (Refs. 25, 26) investigated the effects of FBG integration on the structural properties of composite parts. This investigation included testing small samples with and without FBGs and successfully embedding them into a small-scale blade for static and dynamic testing both in the laboratory and on the MERIT rotor test rig (Ref. 27).

The present work investigates the feasibility and accuracy of reconstructing rotor component loads for usage monitoring using a FBG-instrumented rotor blade. In this context, a pre-series AW09 main rotor blade was equipped with FBG sensors. A test campaign with an instrumented rotor on a full-scale rotor test rig was conducted and provided the basis of this analysis, which establishes a mathematical relationship between load signals on rotor components and the strain signals of the rotor blade.

FBG INSTRUMENTATION

The rotor blade was instrumented – in addition to electrical resistance strain gauges – with a total number of 60 FBG strain sensors at five distinct radial sections, and two FBG temperature probes. The strain sensors were bonded to the outer surface of the rotor blade both in axial direction and in ±45° pairs. The radial distribution was determined from numerical modal analysis to capture at least the first five natural modes of the rotor blade. The four optical fibers with their gratings were placed in the respective quadrants of the cross-section in such way, that under load the strains of each sensor of a fiber usually have equal signs. Each of the two temperature probes was spliced to the end of a fiber and encapsulated by a stainless steel tube for isolation from mechanical strains. One sensor was bonded to the suction side and one to the pressure side of the rotor blade. Figure 1 shows an illustration of the sensor network and fiber routing. The unique sensor indexes refer to the fiber and grating numbers.

The signal processing path from the individual measured Bragg wavelengths to cross-sectional strains, sectional forces as well as rotations and displacements of the rotor blade are explained and validated in detail by the authors in Ref. 28.

An interrogator identified the peaks in the reflected optical spectrum and assigned the wavelength to each dedicated sensor. The local strains were calculated from the change of Bragg wavelength with the knowledge of the gauge factor k, as well as the linear (ζ_1) and quadratic (ζ_2) components of the thermo-optical coefficient. Assuming uniform temperature distribution on each side of the blade, the measurements of the two temperature probes were used to compensate the thermo-optic effect. Sectional strains $\varepsilon_c = (\bar{\varepsilon}_1, \kappa_1, \kappa_2, \kappa_3)$ constitute a primary focus of this study. These strains represent the sectional axial strain $\bar{\varepsilon}_1$, the twist rate κ_1, and the flap and lead-lag bending curvatures κ_2 and κ_3. The *kinematic strain–displacement relation* describes how strain signals measured at sensor location i correspond to the beam's sectional strains.

It is described as a combination of the Euler-Bernoulli beam formulation for the axial strain field, which has been proven to be adequate for isotropic homogeneous beams under extension and bending, together with a calibrated coefficient c_{12}, which relates the local shear strains to the twist rate. The axial entries of the matrix of Equation (1) are defined by the y and z coordinate of the strain sensor.

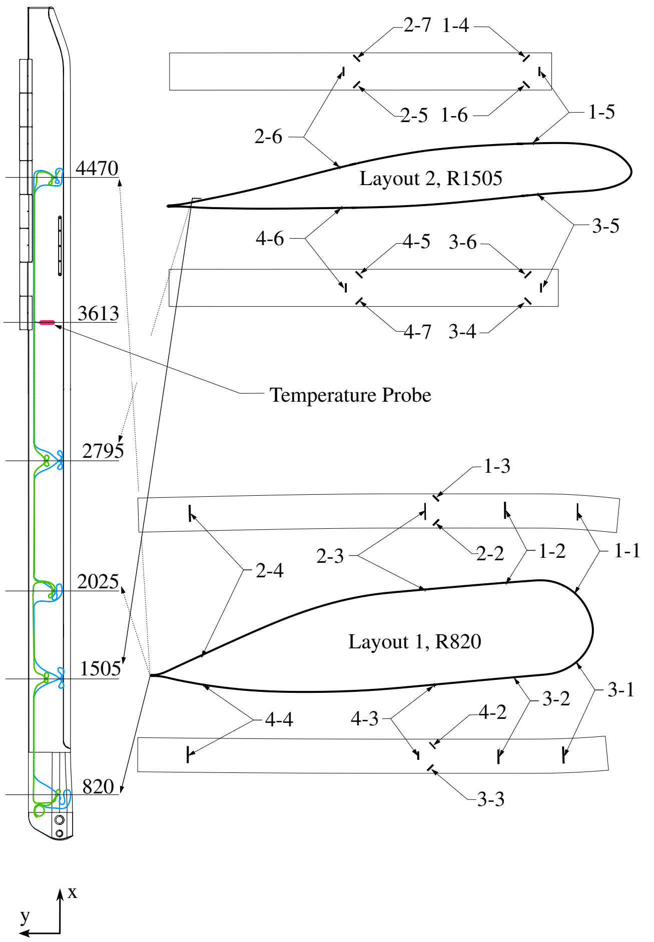

Figure 1. FBG sensor network and fiber routing on a pre-series AW09 rotor blade

$$\varepsilon_c = \begin{bmatrix} \begin{bmatrix} 1 & 0 & z_i & -y_i \\ 0 & c_{12_i} & 0 & 0 \end{bmatrix}_i \\ \cdots \\ \begin{bmatrix} 1 & 0 & z_n & -y_n \\ 0 & c_{12_n} & 0 & 0 \end{bmatrix}_n \end{bmatrix}^{-1} \cdot \varepsilon_i \qquad (1)$$

The derivation and determination of c_{12} as well as the validation of this approach is explained in Ref. 28. This approach was selected due to the fact that the Euler-Bernoulli assumptions provide an inadequate representation of the behavior of beams subjected to torsion. If the beam is twisted, the cross-section warps out-of-plane, which leads to a strain-displacement relationship depending on the partial derivatives of an unknown warping function. In this case, optical deformation measurements from lab tests were used to calibrate the c_{12} coefficients for each shear strain sensor location by correlating the twist rate κ_1 from digital image correlation (DIC) measurements to the FBG strain measurements.

Because sectional strains of the rotor blade can occur not only due to the mechanical loads on the blade, but also due to temperature changes, the sectional strains were divided into components caused by mechanical and thermal influences:

$$\varepsilon_c = \varepsilon_{c_{mech}} + \varepsilon_{c_{therm}} \tag{2}$$

A novel in-field calibration procedure, presented and demonstrated in Ref. 28, allows for the calibration and evaluation of the thermal effects of the anisotropic rotor blade structure, resulting in values for the isolated mechanical sectional strains.

In order to evaluate the cross-sectional strains due to thermal expansion, whirl tower data recorded in non-rotating condition was taken as basis. In this condition, mechanical strains were assumed to be invariant, while temperature readings passed a broad range of values. Changes of sectional strains among the non-rotating data sets could be traced back to thermal effects of the anisotropic blade structure.

A regression was performed in order to determine the relation of sectional strains and thermal conditions. The input parameters were the temperature sensor signals, which could also be preprocessed into their spatial distribution to better represent non-uniform temperature distributions:

$$\varepsilon_{c_{therm}} = f\left(T_{mean}, \Delta T\right) \tag{3}$$

This in-field thermal calibration offers several advantages. It improves thermal compensation accuracy by accounting for the anisotropic thermal behavior and non-uniform temperature distribution within the composite structure, without requiring complex finite element models. Additionally, it reduces costs by eliminating the need for controlled laboratory environments and allows for anomaly detection during repeated recalibration cycles.

The derived sectional strains were directly related to the corresponding sectional loads by multiplication with the predetermined beam sectional stiffness matrix K, as denoted in Equation (4). This matrix captures the beam behavior obtained from laboratory tests, as detailed in (Ref. 28), where applied loads and resulting strains were simultaneously measured.

$$F = K\varepsilon_{c_{mech}} \tag{4}$$

Subsequently, the derived sectional strains underwent further processing to estimate the elastic deflections and overall deformation of the blade. This involved the interpolation of strains between measurement points and the solution of an initial value problem using a quaternion-based rotation representation.

WHIRL TOWER CAMPAIGN

A full-scale whirl tower rotor test campaign was conducted to investigate the relationship between instrumented rotor components and FBG strain signals. Additionaly, the sensitivity of the measured variables to configuration changes and the effect of environmental influences on the signals were evaluated. Figure 2d depicts the configuration of a 64-channel telemetry unit, configured with a sampling rate of 2 kHz. The system acquired the signals of the forces, moments, and displacements of the inter-blade lead-lag dampers, the forces of the pitch links, the forces and moments on the swash plate, blade holder, and rotor mast, as well as local strains of other highly loaded structures. Moreover, signals from blade full-bridge strain gauges were collected to measure bending and torsional moments at five radial sections, providing a comparison with FBG measurements. Additionally, the rotational speed of the rotor, as well as the control variables and the positions and forces of the actuators, were measured. The AeroMini interrogation unit, shown in Figure 2c, and its battery power supply were attached via stud bolts above the telemetry unit. It stored the data with a sampling rate of 500 Hz on an internal SD card. Data synchronization between the two systems was enabled by hammer taps at the beginning and the end of each measurement run. Following data synchronization, cleaning and downsampling the different measurement systems to 500 Hz, the data were unified into a common format. Subsequently, strain and temperature information extracted from FBG sensor were converted into cross-sectional strains and loads using the previously described method.

A total of twelve test runs were carried out, consisting of a shakedown run, four track and balance runs with minor pitch link adjustments and modification of balance weights. This was followed by collective, cyclic control and rotational speed sweeps, a cyclic oscillating (stick-whirl) excitation and a collective oscillating excitation.

Rotor Track and Balance After instrumenting one blade with FBGs, it was statically pre-balanced to take into account the additional weight and to facilitate the subsequent dynamic balancing procedure. Within the scope of the project, dynamic balancing and adjustment of the tracking was not only considered as a preparatory measure, but as an actual test. Changes were induced by modification of balance weights on the rotor head and the adjustment of individual pitch link lengths.

RPM Sweep The objective of this test was to generate a comprehensive database for various rotational speeds. A range of rotational speeds was tested for each collective control angle. Each test condition was kept for 30 seconds, so that a quasi-stationary behavior could be achieved and measured. The transition between the test conditions was smooth. The cyclic setting was kept in a neutral position.

Collective and Cyclic Sweep This test also served to generate a comprehensive database for various operating points with incremental changes to the collective and the cyclical control angles. The transition between the test conditions was smooth, avoiding impulsive parameter changes. Each test condition was kept constant for 30 seconds to allow all parameters to stabilize. The cyclic control angles were specified in different longitudinal and lateral directions at different collective settings.

(a) AW09 rotor test rig

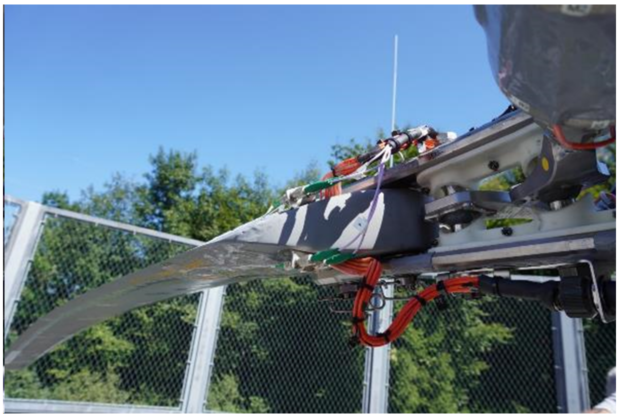

(b) Instrumented pre-series AW09 rotor blade

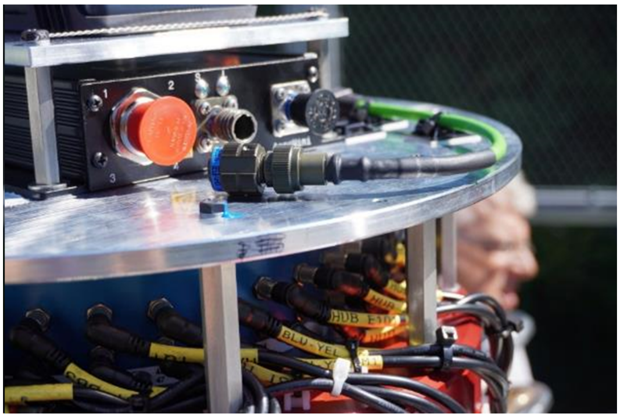

(c) AeroMini interrogation unit

(d) Rotor telemetry, interrogator and power supply

Figure 2.

Cyclic and Collective Oscillating Control Input First, the rotor was dynamically excited by a cyclically oscillating control input with a frequency between 0.5 and 3.2 Hz, a phase offset of $\pm 90°$ between lateral and longitudinal cyclic and an amplitude of $1°$. Subsequently, the collective controls were also excited with frequencies between 1.5 and 3 Hz and an amplitude of $1°$. An essential goal of this study was to assess the motions and loads at the damping elements due to the excitation of the lead-lag modes.

METHODOLOGY

This paper presents an analysis of different methods and results for the previously introduced regression problem, with the aim of determining the loads on different rotor components (e.g. inter-blade damper, pitch link, and mast bending moment) based on the measured variables from the rotor blade. Figure 3 illustrates the data processing, training and evaluation pipeline of this study.

Data Preparation

The initial stage of the data preparation process comprised the extraction of individual rotor revolutions, facilitated by the rotary encoder signal. The input features for the supervised regression problem were the sectional strains of the rotor blade including the sectional axial strain $\bar{\varepsilon}_1$, the twist rate κ_1, the flap-bending curvature κ_2 and the lead-lag bending curvature κ_3 for each of the five instrumented cross-sections, as well as the mean and delta of the rotor blade temperature probes (T_{mean}, ΔT), the rotational speed Ω, and the collective and cyclic control inputs ($\theta_0, \theta_s, \theta_c$). In this study, the target variables were the pitch link force F_{pl}, the aft inter-blade damper force F_D and the longitudinal mast bending moment M_y. The input vector was constituted by the mean value of the control inputs and the temperatures per rotor revolution, as well as the harmonic decomposed signals of the rotor blade, which consisted of the first 20 real and imaginary parts of the discrete Fourier transform. This resulted in an input vector size of 786. Furthermore, the rotor revolution of the three target variables was also decomposed into its first 20 Fourier coefficients, resulting in an output vector size of 117. The data set was then transformed into a standardized scale with zero mean and a standard deviation of one.

Supervised Regression

The data was split into a subset for training (*training set*), hyperparameter tuning and cross-validation (*development set*), while another, non-overlapping subset of data was used to evaluate the performance of the model (*test set*). According to

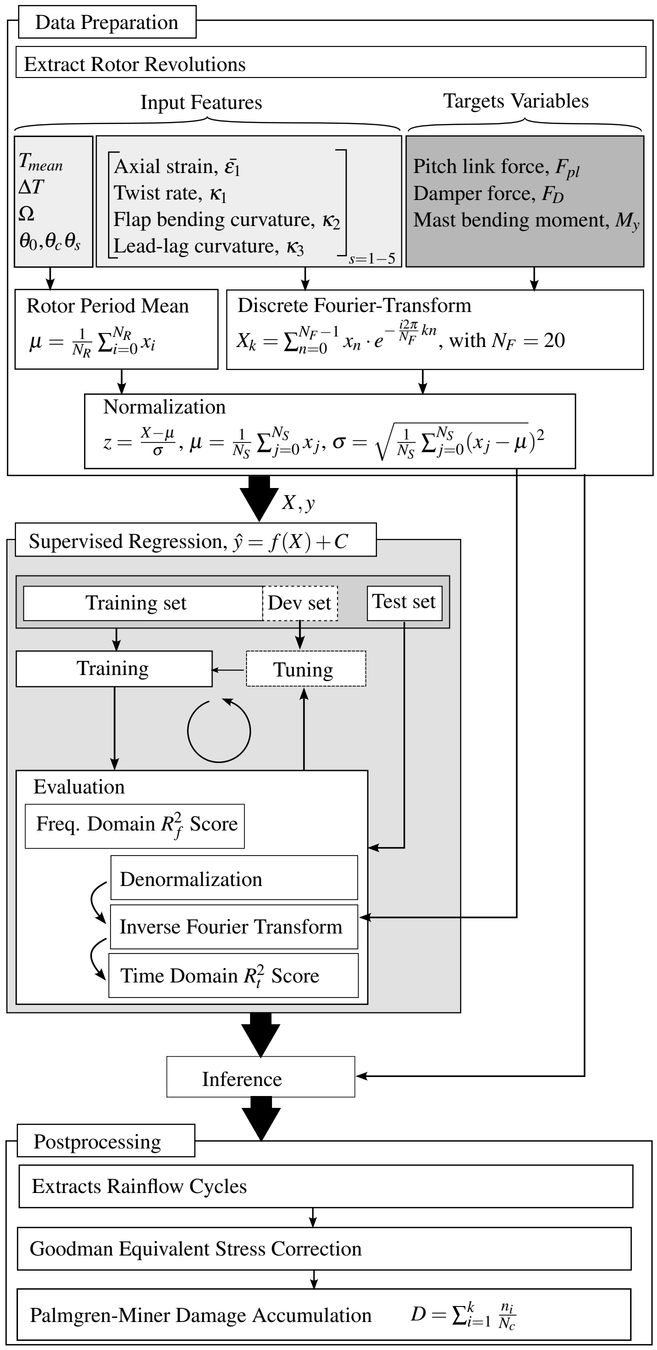

Figure 3. Flowchart

the described data preparation, each rotor revolution created a single sample in the data set. Each of the splits allocated 75% of the data to the training data set and 25% of the data to the test data set.

Because the measurement campaign provided only a limited and imbalanced data set in terms of the distribution of rotor states, a stratified shuffle split was used to preserve the percentage of samples for each class (rotor controls and rotational speed) in both the training, development and test sets. Each type of actuation input was classified to represent different rotor states, e.g. non-zero cyclic input or below nominal speed RPM. It is important to note that there was a possibility that the method did not provide sufficient independence between the training and test data sets, because subsequent rotor revolutions were likely to contain similar information. Nevertheless, in the present context, the division of grouped individual test runs was deemed to be an unsuitable approach, as it resulted in significantly different distributions of test and training data sets.

This study examined the performance of a linear relationship (linear regression) between the input and output features and compared it to that of an artificial neural network (ANN), which is capable of identifying non-linear relationships within the data.

Both the linear regression and the ANN tried to minimize the least squares error of the 117 Fourier target variables. While the solution for the linear-regression was straight forward, a hyperparameter search (tuning) was conducted for the ANN to find a set of external model parameters to maximize its performances. The model performance was evaluated with the coefficient of determination for the mapping of the Fourier coefficients (R_f^2) but also by re-transformation and evaluation in the time domain (R_t^2).

Postprocessing

In order to evaluate the suitability for load monitoring, rain flow cycle counting was used to extract fatigue-relevant information from the complete time-history signal of the target variable signals. Local minima and maxima were determined and cycles were iteratively identified and removed in a form that resembles raindrops falling on a roof. These cycles were characterized by their amplitude and mean. To prevent artificial discontinuities in the time signal introduced by data splitting, the entire time series was subjected to inference using the previously determined regression model. The subsequent Goodman correction adjusted the alternating loads of a cycle into an equivalent load based on its mean to account for the effect of mean load on fatigue strength. The implementation was based on Ref. 29, 30. The calculated equivalent loads were then put into a Palmgren-Miner linear damage accumulation model, together with a generic S-N curve, in order to estimate the damage caused by each cycle and to derive a scalar metric for the suitability of the load regression task for load monitoring.

RESULTS

This study investigates the potential for predicting loads on key rotor components, namely the pitch-link force F_{pl}, the mast bending moment M_y and the aft inter-blade damper force F_D, based on the previously described FBG instrumentation of the rotor blade. In the majority of the presented results, and unless otherwise stated, linear regression has been used. Additionally, this approach was compared to an artificial neural network approach.

A description of the whirl tower test data used for this regression in terms of control inputs can be found in Figure 4.

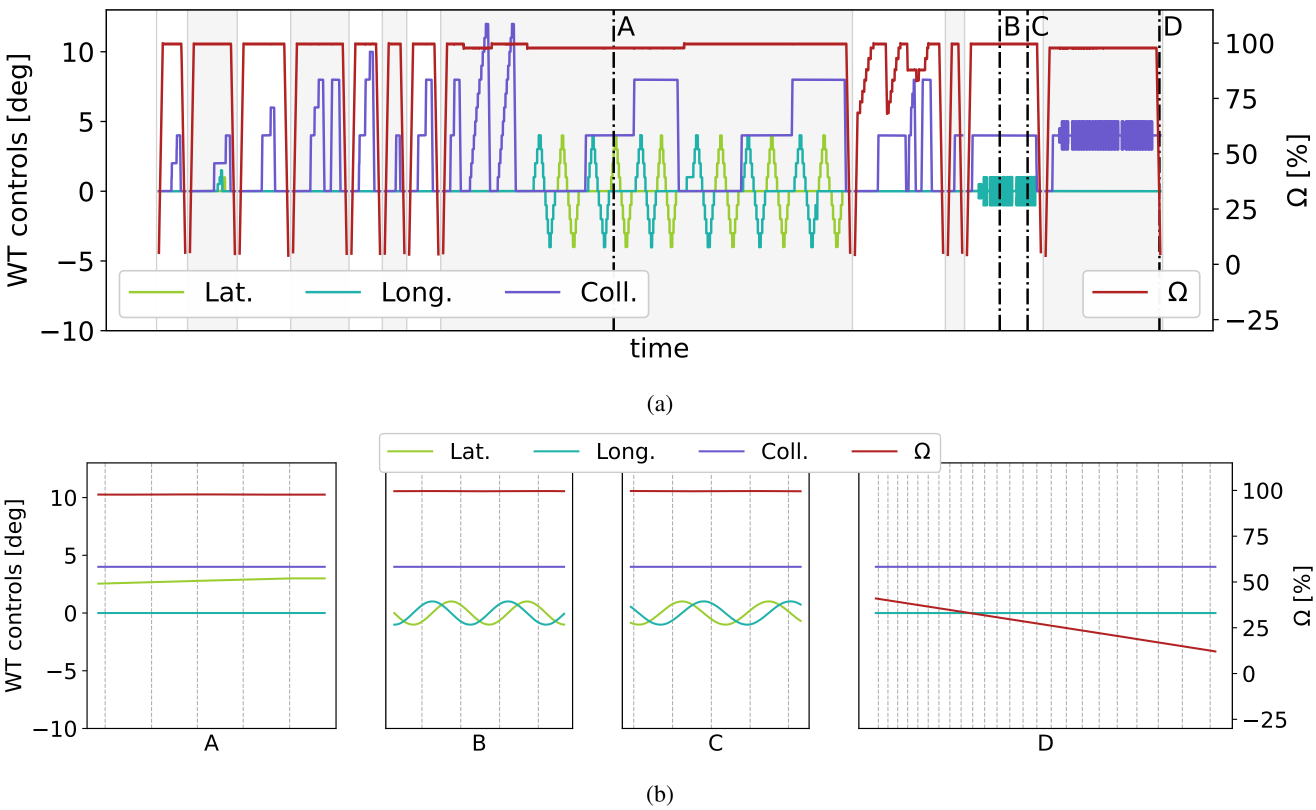

Figure 4. Whirl tower control inputs. (a) Complete test campaign; all individual test runs are indicated by the gray shading. (b) Selected sequences for detailed analysis; rotor revolutions are indicated by the gray dashed lines.

In addition to the blade pitch control (collective, longitudinal cyclic, lateral cyclic), the rotational speed Ω is also encompassed in the following when referring to *rotor controls*[θ]. Figure 4a gives an overview of the concatenation of all test runs. In order to better assess the agreement of the signals on a more detailed level, some small subsections of such tests were selected for all comparisons in the following work. These subsections are labeled A to D (see Figure 4a) and are shown in Figure 4b. Section A describes a baseline case with slowly varying control inputs, including collective and cyclic control. Sections B to D represent special cases with challenging conditions. Sections B and C include fast periodic changes of the cyclic controls, but with different phase and frequency. Section D represents the deceleration phase of the rotor, including a highly nonlinear response. The dashed lines mark the point at which a full rotation of the rotor is completed.

Signal Reconstruction from Truncated Fourier Series

To reconstruct the load signal of rotor components using data from the instrumented blade, a Fourier-based approach was employed. The method involves transforming time-domain signals into the frequency domain to extract essential characteristics. A model is then trained to predict Fourier coefficients of target sensors based on those from the instrumented blade. Finally, inverse Fourier transformation and fatigue assessment metrics (e.g., rainflow counting and Miner's rule) are applied to quantify component accumulated load history. A detailed overview of this process is visualized in the flowchart of Figure 3 presented in the previous section. This transformation pipeline assumes predominantly periodic rotor behavior. For non-periodic rotor states, accurate signal representation requires a large number of Fourier coefficients, especially at the transition from one rotor revolution to the next.

Figure 5 illustrates the impact of harmonic truncation on the R_t^2 score, which quantifies the agreement between the inverse-transformed, truncated FFT signal and the original signal. For a perfect match of the signals, 40 or more harmonics (N_F) are required, except for the mast bending moment where fewer harmonics were sufficient. However, for the following analysis, it was assumed that the high frequency content is less relevant to load-monitoring and may also contain a relevant amount of noise. Therefore, 20 terms in the Fourier series (N_F) were considered sufficient for the following task. To assess the performance of the regression, the Fourier-transformed signal (containing 20 terms) served as the reference for subsequent analyses, with the R^2 value used as an evaluation metric. Additionally, the high R_t^2 value of over 0.98 achieved with only a few harmonics strongly suggests that the analyzed signal exhibits a high degree of periodicity and can be effectively represented using a limited number of Fourier components.

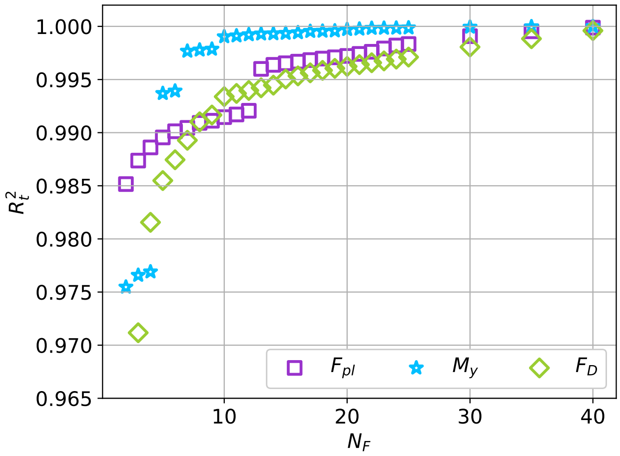

Figure 5. Coefficient of determination (R^2) evaluated between the measured signal and the signal resulting from the Fourier transform and the inverse Fourier transform (applied on full rotor revolutions) for a range of Fourier series terms N.

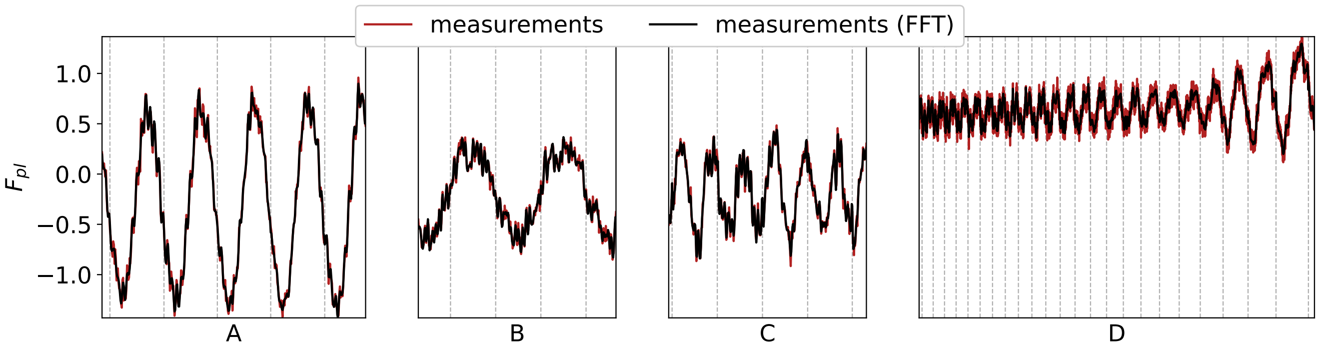

Figure 6. Comparison of the pitch link force over time between the measured signal and the signal resulting from the Fourier transform and the inverse Fourier transform ($N_F = 20$) in segments A to D.

Figure 6 compares the original pitch link force signal and the Fourier transformed signal (20 terms in the Fourier series) in the time domain based on the previously described time series A to D. Sections A to C show similar good agreement. Section D shows slightly more deviation. This is due to the fact that longer time series (significantly reduced rotor speed) are described with the same number of terms in the Fourier series.

Feature Importance Analysis - Sectional Strains

The following analysis aims to determine the relative contributions of input features to the accuracy of the regression model. As described earlier, the original signals from the FBG sensors were preprocessed and transformed into blade sectional strains at five distinct radial sections. The signals used as input features for the regression model are the sectional axial strain $\bar{\varepsilon}_1$, the twist rate κ_1 and the flap and lead-lag bending curvatures κ_2 and κ_3. Figure 7 shows how the result is affected when only certain (combinations of) input features are used to estimate the target sensor signals. The error bars refer to a four-fold cross-validation of the results, with 75% of the data assigned to the training set and 25% of the data assigned to the development set. The variation in the result due to the different data splits was generally small, as indicated by these error bars. It should be noted that the R^2 values presented in this figure and in subsequent analyses were calculated using the test set, which was not employed in the model training process.

The symbol θ is representative for all control inputs including the rotor speed in this analysis. It shows that with such control parameters, the regression performs inappropriately in terms of the Fourier coefficients of the signal. However, in the time domain there is reasonable performance at least for the pitch link force and the mast bending moment. This shows that the main characteristic of the signal in terms of the mean and first harmonic is probably adequately represented by this type of regression, but the higher harmonic content is not adequately

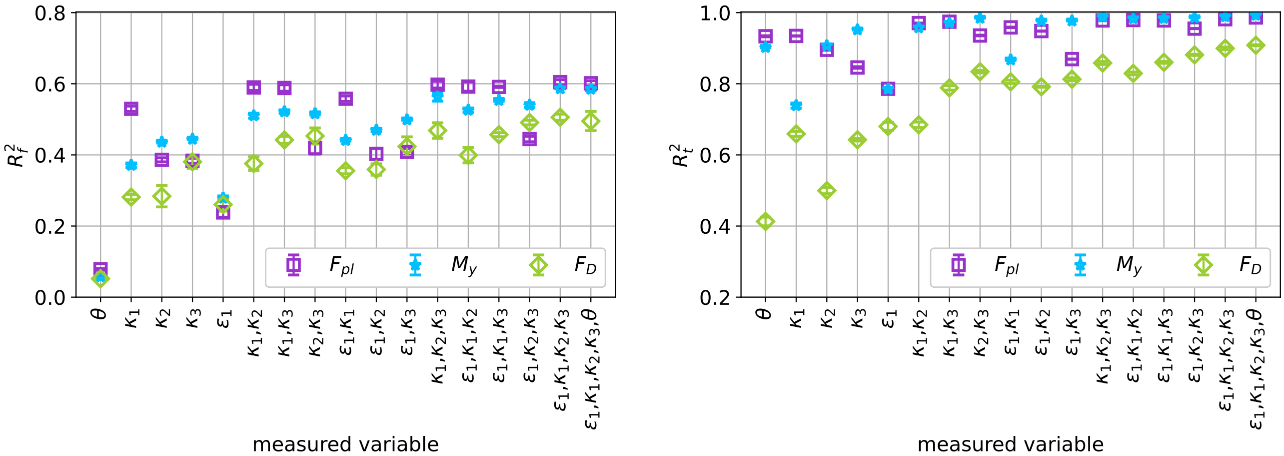

(a) frequency domain

(b) time domain

Figure 7. Coefficient of determination (R^2) between reference signal and prediction for a variation of the physical feature variables. Error bars relate to a cross-validation study with four different data splits.

represented.

Furthermore, Figure 7 shows the trend that the regression improves with a higher number of FBG signals. The model with the highest number of input features, namely the combination of FBG sensors and control inputs, exhibited a relatively modest benefit from the utilisation of the aforementioned controls as additional feature variables. Figure 7 also indicates that the twist rate κ_1 is the most influential factor affecting pitch link loads, while the bending curvatures κ_2 and κ_3 are critical for the mast bending moment and inter-blade damper forces. The graph also indicates that the performance was poorest in the context of the inter-blade damper force.

Figure 8 shows a comparison between the load regression based only on the rotor control inputs and the load regression based on all available feature sensors (FBG + controls). It confirms that for the case A, the controls already resulted in a reasonable agreement between measured and predicted signal. However, the performance of the prediction deteriorates considerably for the more complex cases. In particular, during the rotor deceleration phase and with oscillating cyclic control inputs (compare F_D in B and C). While control variables alone are not suited to accurately predict the target signals, incorporating FBG sensors significantly improved the predictive performance.

Figure 9 compares two cases representing different levels of complexity of the FBG instrumentation. The case where the twist-rate κ_1 was not used during the regression would allow a less complex architecture of only axial FBG sensor orientation without the need for shear strain measurements. It is compared to the case where all feature variables of the FBG instrumentation (including κ_1) were used. In most cases, the difference was marginal and the benefits of this sensor system would be largely available with the simpler instrumentation. However, some benefits were found in the pitch link force and in the more complex scenarios, especially during the rotor deceleration phase.

Feature Importance Analysis - Radial Position

Subsequent to the analysis of physical variables (as detailed in the preceding section), the influence of the number and location of the instrumented FBG sections is investigated below (see Figure 10). For practical reasons, a simplified indexing of the FBG instrumented radial stations is used in this part of the paper. The indices range from 1 – most inboard radial station R820 – to 5 – most outboard radial station R4470.

In the frequency domain, the performance of the regression is slightly dependent on the radial station, and the trend is somewhat indistinct. This ambiguity is most likely related to the relative position of the instrumented section to the mode shapes of the rotor blade Apart from that, it shows again that the prediction improves with more sensor data, in this case instrumented radial stations.

Time-domain analysis reveals that incorporating the most inboard section (1) yields the most accurate predictions of mast bending moment and inter-blade damper force. In fact, this section can provide a good estimate of these loads when employed on its own.

The placement of the sensor in a more outward position resulted in a notable deterioration in the quality of the prediction. Conversely, the pitch link loads exhibited a lack of discernible pattern with regard to radial positioning, even when examined in the context of time-series data.

A detailed view of the predicted time signal for two different types of instrumentation is shown in Figure 11. The first scenario is defined by using only the innermost FBG instrumented radial station. The second scenario is defined by using

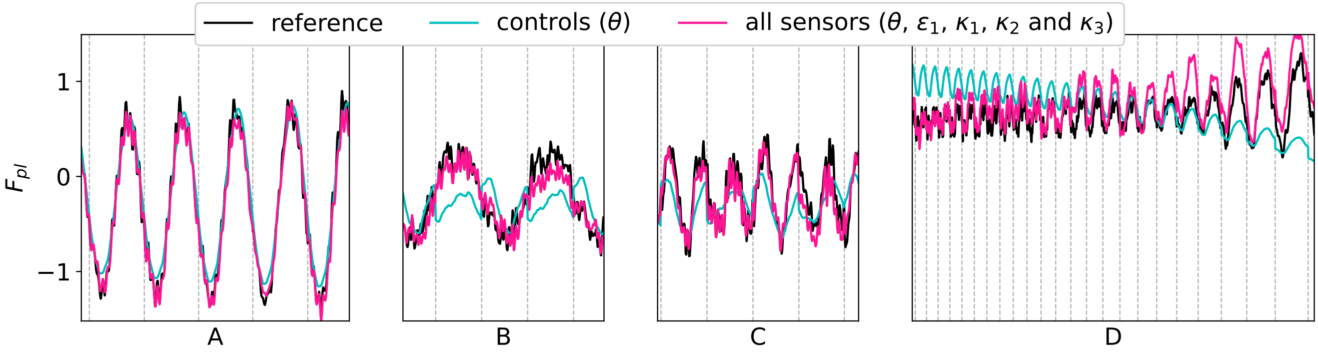

(a) Pitch link force (F_{pl})

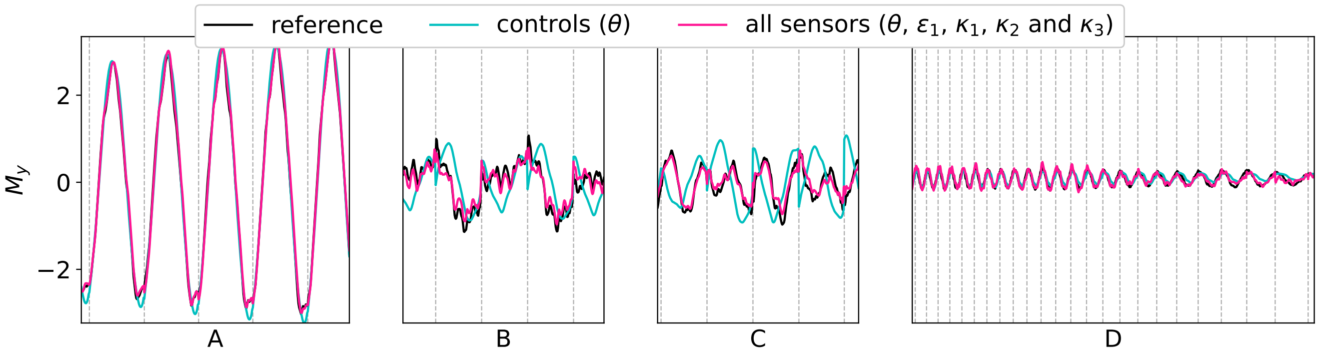

(b) Rotor mast bending moment (M_y)

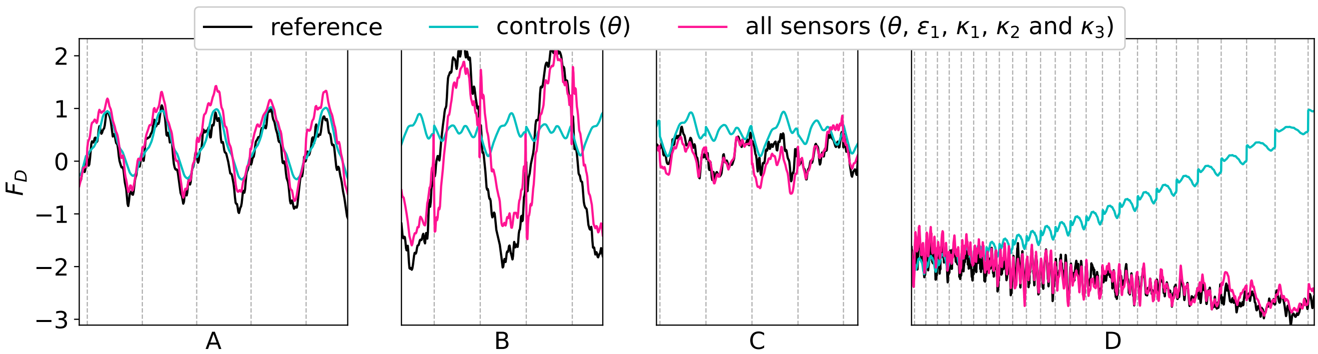

(c) Inter-blade damper force (F_D)

Figure 8. Comparison of the measured and predicted time signals in segments A to D. Predictions based on the rotor control inputs as the only feature variables compared to the case where all sensors (controls and FBG sensors) were used as feature variables.

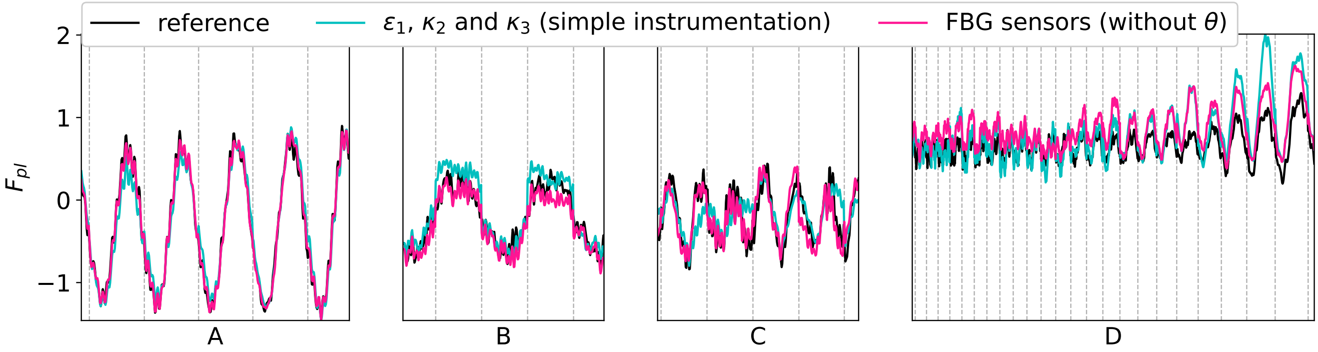

(a) Pitch link force (F_{pl})

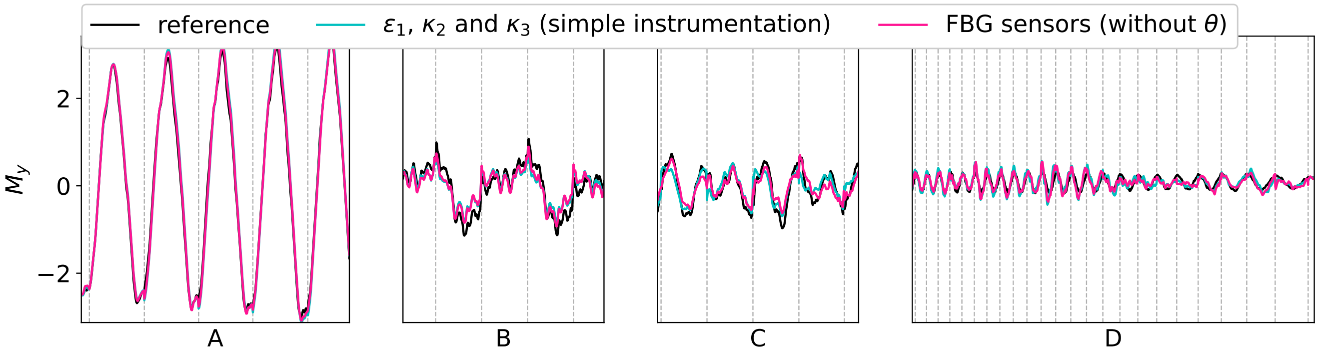

(b) Rotor mast bending moment (M_y)

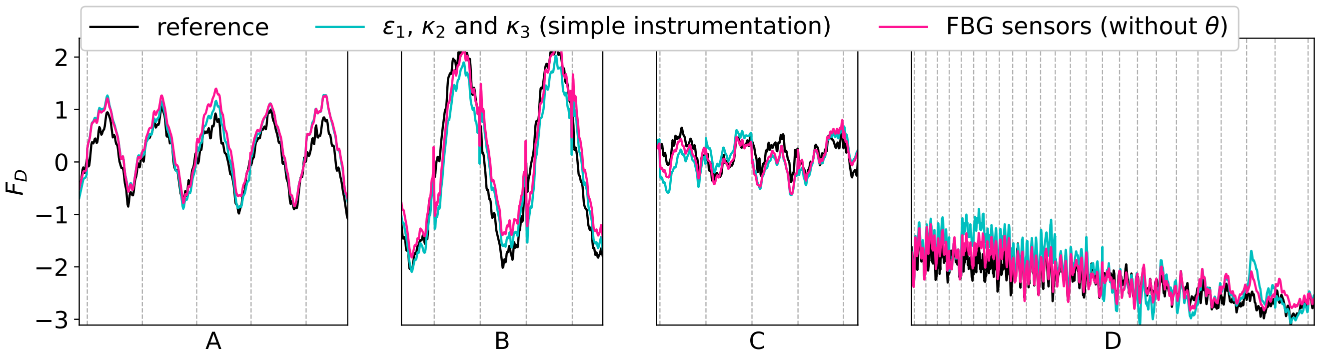

(c) Inter-blade damper force (F_D)

Figure 9. Comparison of the measured and predicted time signals in segments A to D. Predictions based on different levels of complexity in terms of blade instrumentation.

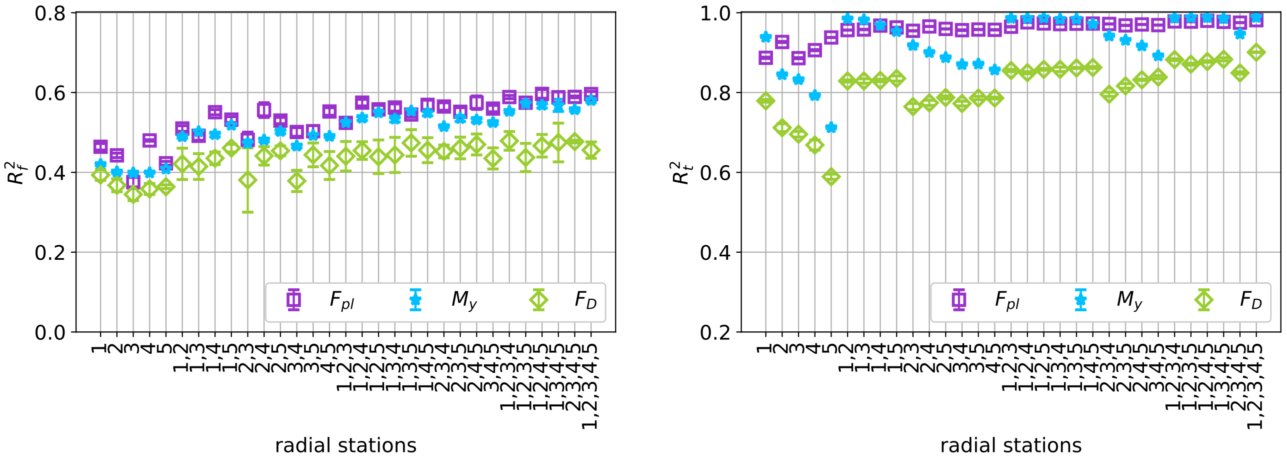

(a) frequency domain

(b) time domain

Figure 10. Influence of different sensor positions along the rotor blade (from 1 – most inboard – to 5 – most outboard) on the performance of the load regression. Error bars relate to a cross-validation study with four different data splits.

an additional section, i.e. the signals at radial station number four. In both cases, the baseline case A is well predicted. For the special cases, the performance of the prediction ranges from reasonable to good, with a moderate improvement due to the additional sensor at radial station number four. This further illustrates that even a basic blade instrumentation system has the potential to be effective in this particular application.

However, there are some noticeable deviations between the reference signal and the predicted signal, especially during the rotor deceleration phase. This was already the case in previous comparisons, e.g. Figure 8. It was ascribed to the occurence of very similar states in terms of feature sensors, but notably different states in terms of the output sensors, e.g. due to resonance in certain components. However, due to the reduced number of variables, the model is not able to sufficiently differentiate such conditions, which are similar in terms of inputs, but still significantly different in the response of the system. This problem is aggravated by the small number of rotor acceleration and deceleration occurrences in the data set, combined with certain resonances that are typically encountered when passing through this frequency range. Increasing the number of feature variables used in the regression and the amount of training data increases the chance of successfully differentiating such conditions.

Linear Regression vs. Neural Networks

Neural networks offer promising possibilities in the area of regression tasks with complex functional dependencies, including the prediction of time signals based on appropriate input data. Accordingly, the following analysis compares the performance of neural networks with that of the presented linear regression.

The architecture of the neural network is of central importance for the quality of results. For this reason, a grid search hyperparameter optimization is carried out. In particular, the number of hidden layers, the number of neurons per layer and the learning rate are varied. For both the input and the output layer, a linear activation function was used, while the hidden layers were based on the PReLU activation function. Figure 12 shows the results of the hyperparameter tuning in the form of a parallel coordinates plot. It visualizes the relationship between hyperparameter values and model performance. The performance metric shown on the right hand side is the mean value of the R^2 scores of the three target variables in the frequency domain. Shallow neural networks with two to three hidden layers and a moderate number of neurons (HL1-HL3) achieved the best performance. Optimal results were obtained using a constant learning rate within the range of $1 \cdot 10^{-3}$ to $5 \cdot 10^{-3}$. Increasing the complexity of the network through additional layers or neurons did not yield further performance gains.

A comparison between the neural network and the linear regression in terms of predicting the target sensor signals is presented in Figure 13. The neural network demonstrates superior performance in the frequency domain, as indicated by a higher R_f^2 score. Conversely, linear regression achieves a better R_t^2 score in the time domain.

The discrepancy was thought to be due to the fact that the mean deflection and low frequency harmonics were underrepresented by the score metric used to train the model, i.e., an evaluation of the R^2 value on all Fourier coefficients. Instead, this approach weighted all harmonics equally. Thus, the behavior obtained is similar to ordinary overfitting, but instead of overfitting on the training data set, the overfitting concerned the score metric, which does not perfectly describe the specific demands of this study.

Accordingly, there was less good agreement between the ref-

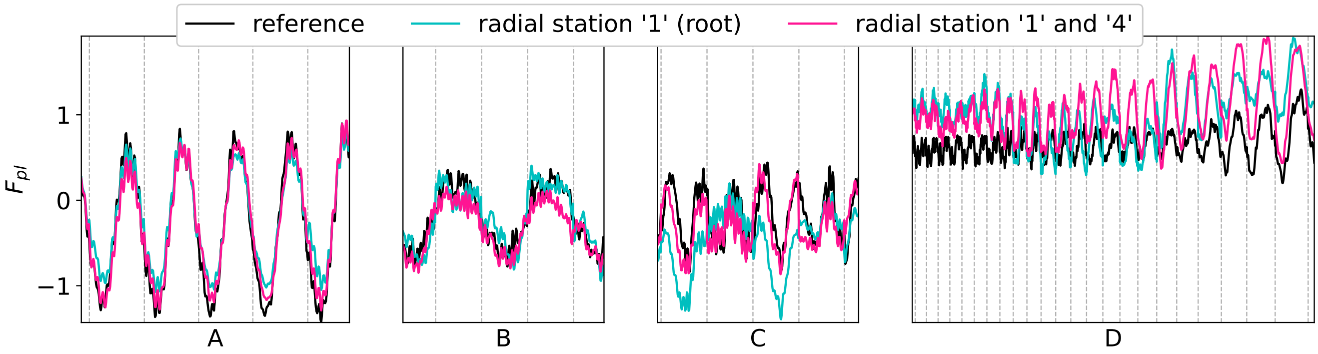

(a) Pitch link force (F_{pl})

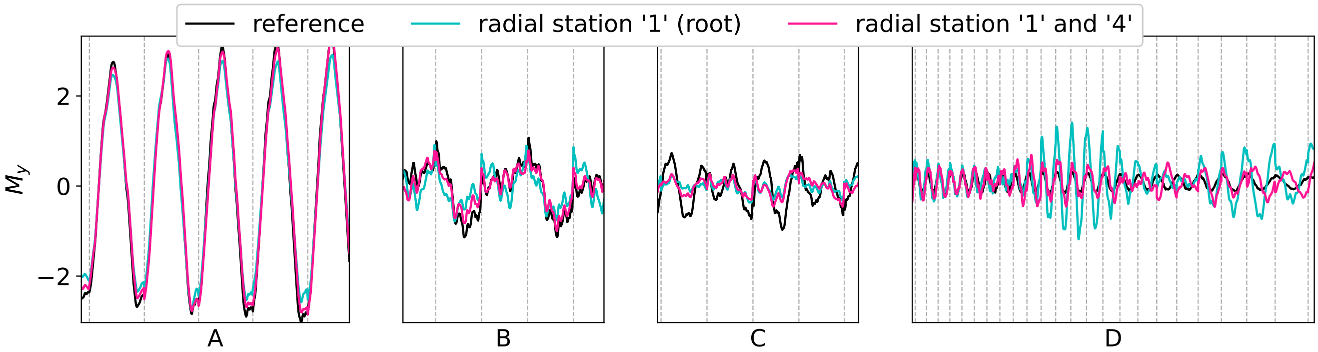

(b) Rotor mast bending moment (M_y)

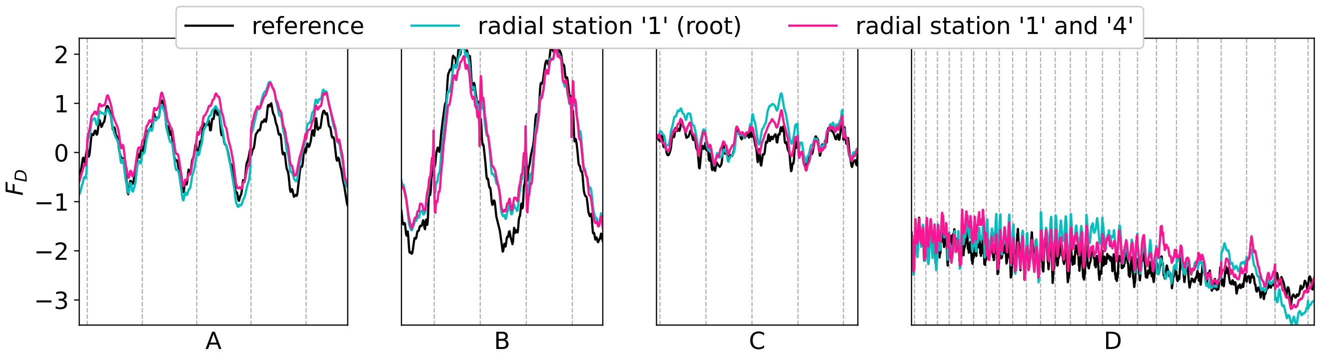

(c) Inter-blade damper force (F_D)

Figure 11. Comparison of the measured and predicted time signals in segments A to D. Predictions based on FBG sensors being placed at specific radial stations only.

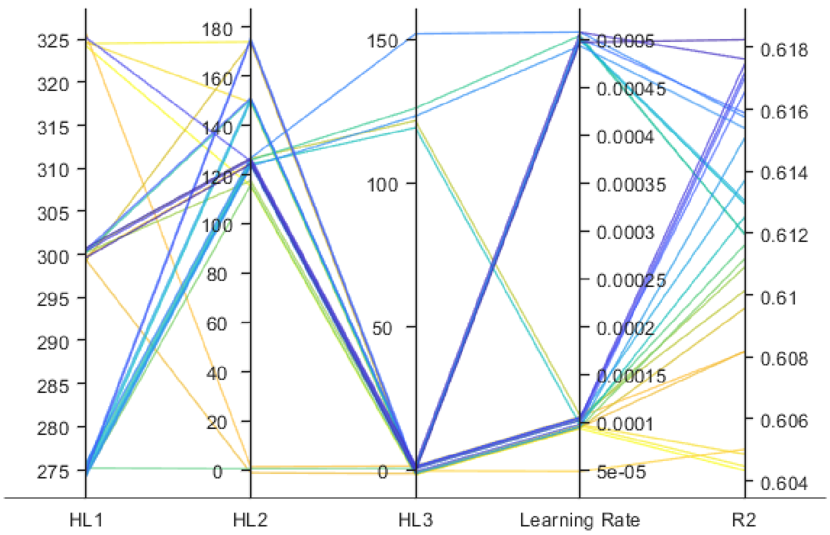

Figure 12. Hyperparameter tuning of the neural network.

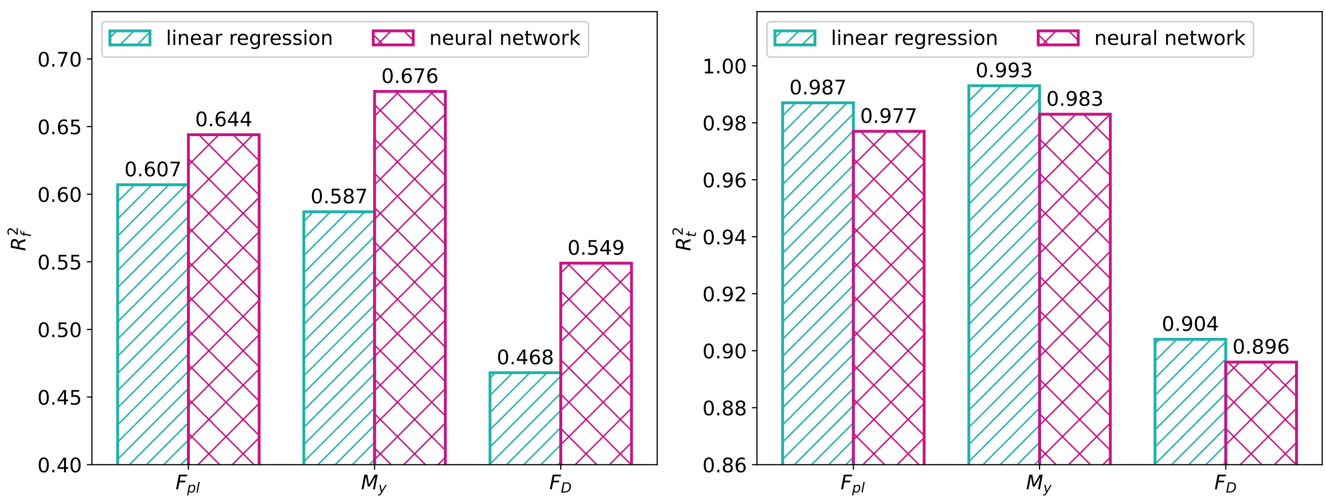

(a) frequency domain (b) time domain

Figure 13. Coefficient of determination (R^2) between reference signal and prediction. Comparison of linear regression and neural network.

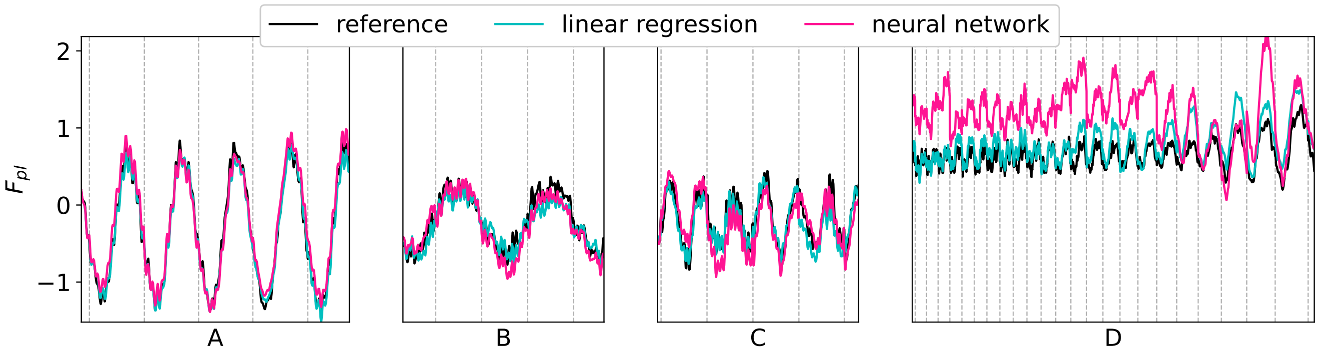

(a) Pitch link force (F_{pl})

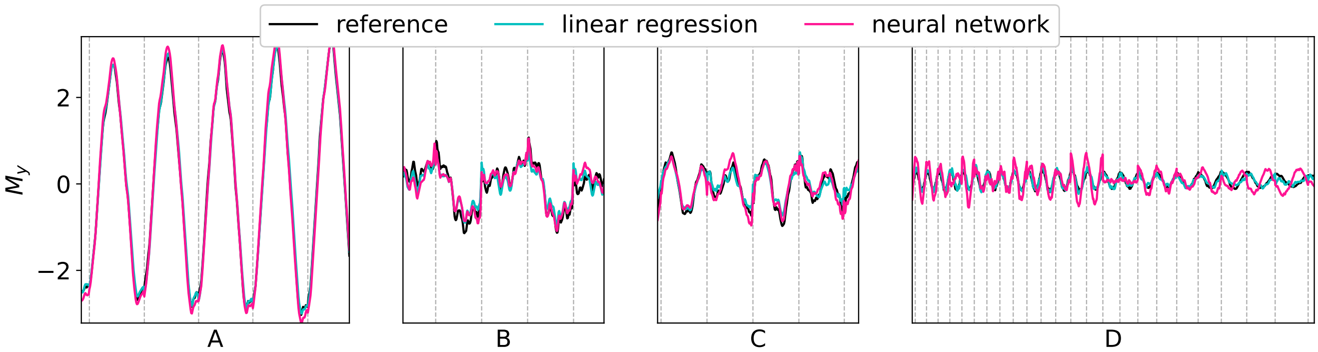

(b) Rotor mast bending moment (M_y)

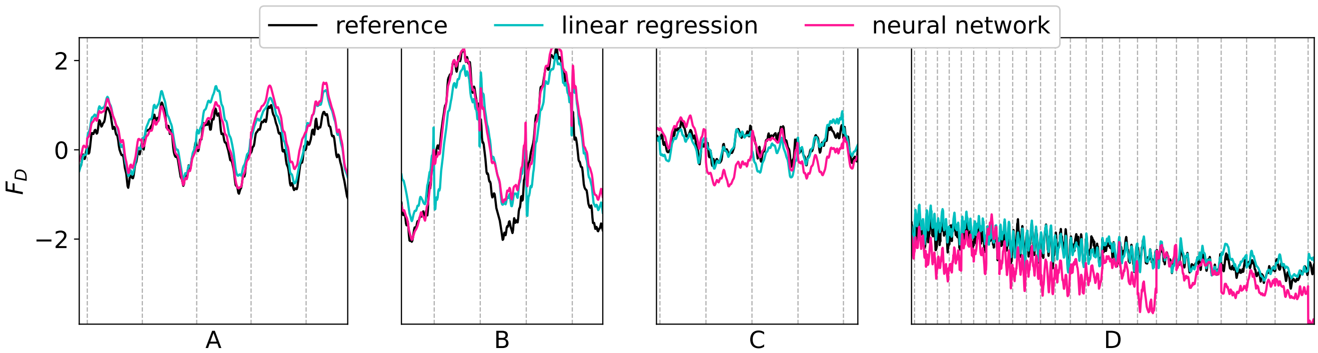

(c) Inter-blade damper force (F_D)

Figure 14. Comparison of the time signal predictions (segments A to D) of a linear regression and an artificial neural network.

erence signal and the signal predicted by the neural network (see Figure 14). Although the prediction was quite similar for most of the sequences monitored, the performance of the neural network was not satisfactory, especially during the rotor deceleration phase.

Therefore, artificial neural networks (ANNs) are a promising approach to rotor load prediction for monitoring applications. However, further research is necessary to enhance their accuracy. This could be achieved by employing a more suitable loss function. Additionally, the availability of larger and more diverse datasets would be instrumental in improving the overall performance of these models.

Fatigue Evaluation

This section evaluates the applicability of this approach for load monitoring by extracting and analyzing fatigue-relevant data as outlined flowchart in Figure 3 in the methodology section. Figure 15 presents rainflow amplitude distributions for the three target components. The pitch link force and rotor mast bending moment exhibit excellent agreement with the reference data. In contrast, the inter-blade damper shows less accurate results, particularly in the high load region.

This region of the inter-blade damper was assumed to be significantly influenced by the acceleration and deceleration phase of the rotor, where resonance frequencies are passed. The inappropriate prediction of this regime may be related to the particular sensitivity of the inter-blade damper force to such resonances in the rotor system.

In this study, the Palmgren-Miner rule, combined with a suitable and in this case generic S-N or endurance curve, is employed to weight load cycles based on their equivalent load. This approach yields a scalar metric for assessing the regression model's ability to predict damage-inducing load cycles. The relationship between the endurance curve and the rainflow count is shown in Figure 16.

The final result in terms of an accumulated damage of the monitored components is shown in Figure 17. The rotor mast bending moment exhibits excellent agreement with a deviation of less than 2%. In contrast, the agreement for pitch link forces and inter-blade damper forces is significantly lower. When comparing the results of the pitch link force and the inter-blade damper, the difference does not match the impression from Figure 15, where the characteristics of the pitch link force were better represented than those of the damper. One reason for this could be the fact that discrepancies in the rainflow count can be compensated when calculating the accumulated damage. Therefore, inappropriate time signals may result in a good fatigue prediction. Another influence that is not covered by the rainflow cycle count and could therefore

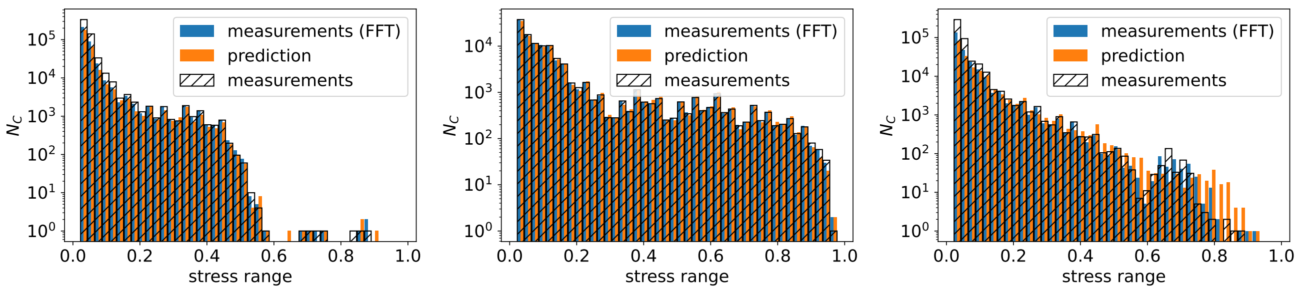

(a) Pitch link force (F_{pl}) (b) Rotor mast bending moment (M_y) (c) Inter-blade damper force (F_D)

Figure 15. Comparison of the rainflow amplitude range count applied to the measured and predicted signals for all three target rotor components.

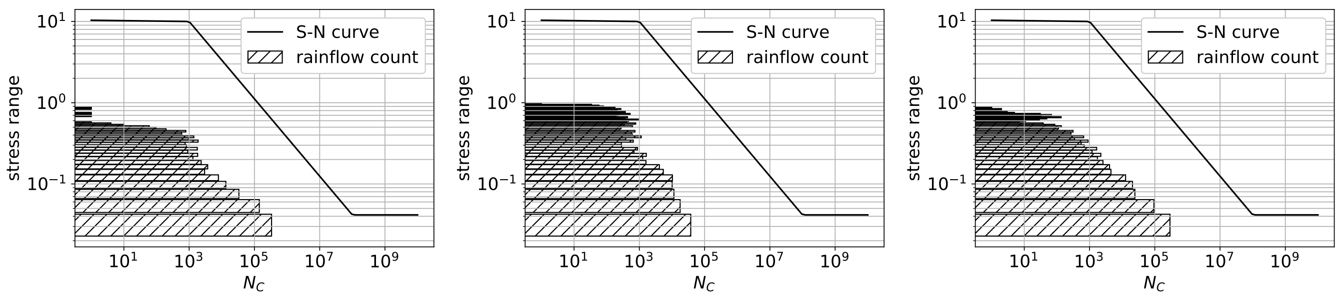

(a) Pitch link force (F_{pl}) (b) Rotor mast bending moment (M_y) (c) Inter-blade damper force (F_D)

Figure 16. Generic S-N curves for all three rotor components in relation to the rainflow count.

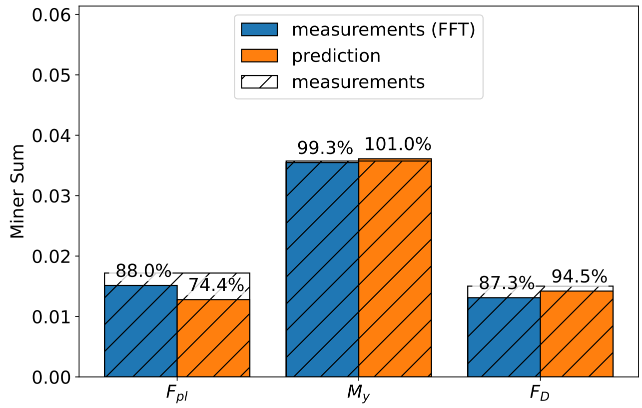

Figure 17. Linear accumulated damage

explain this phonemon is the effect of mean load, which is part of this final processing.

One potential explanation for this is that discrepancies in rainflow cycle counting can be offset during accumulated damage calculation, leading to accurate fatigue predictions even with inaccurate time signals. Additionally, the influence of mean load, which is considered in the final processing, is not shown in the Figure 15 and could contribute to this phenomenon.

Overall, all the metrics presented to assess the performance of the regression are not sufficient to be used in isolation, but need to be evaluated together for a reliable judgement.

CONCLUSION

This study presented a methodology for predicting the pitch-link force, mast bending moment, and inter-blade damper force using data from a fiber Bragg-instrumented pre-series AW09 rotor blade. Data from a full-scale whirl-tower test campaign was used to correlate the rotor component loads with strain signals. Time-domain data was transformed into frequency-domain features to train a supervised regression model predicting target load sensor Fourier coefficients. To evaluate the impact of specific blade instrumentation characteristics, including local deformation and sensor radial position, on model performance, a linear regression analysis was performed. Additionally, a neural network model was compared to that of the linear regression. The following conclusions were drawn from this analysis:

1. Instrumented rotor blades can be used to estimate the loads of other rotor components.
2. Compared to a regression based solely on rotor control inputs and operating states, the instrumented blades improved the prediction significantly.
3. The results improved as the number of instrumented radial stations increased.
4. The blade signals far inboard tended to be more important than the signals far outboard.
5. A linear regression model was sufficient to to estimate the major characteristic of the load history of the target components.
6. Using neural networks instead of linear regression resulted in a better fit of the score metric used, but not in a better estimate of the time history and fatigue values. However, additional benefits are expected if applied to a rich real-world dataset and if a more suitable loss function is used during training.

The prediction of rotor component loads from blade sectional strains demonstrated promising results for future usage monitoring applications. Our observations indicated that a linear relationship between the Fourier coefficients proved to be an effective solutions for the aforementioned problems, offering a computationally tractable and understandable alternative to potentially more complex and resource-intensive neural network approaches. However, further exploration using real-world application datasets from flight test data is crucial to solidify these findings and to assess the generalization of this approach to more complex scenarios.

AUTHOR CONTACT INFORMATION

Tobias Pflumm: tobias.pflumm@koptergroup.de
Dominik Komp: dominik.komp@koptergroup.de
Benedikt Sosa: benedikt.sosa@tum.de
Zeynep Bilgin: zeynep.bilgin@tum.de
Andreas Jochum: andreas.jochum@koptergroup.de
Sören Süße: soeren.suesse@koptergroup.de

ACKNOWLEDGMENTS

This work was supported by the Bavarian ministry of economic affairs, regional development and energy (StMWi) through the Bavarian research program BayLu25 in the project iRoB as well as through the German federal ministry for economic affairs and climate action (BMWK) though the aviation research program LUFO VI-3 in the project BIGROHU. The authors would like to thank the Kopter component testing department for their incredible support during the project, in particular Slawomir Wybranski, Michael Gallo, Max Volk, Max Hönig, Giuseppe Bonanno, Marc di Guisto, Pietro Zugnoni, Federico Savorgnan, Safoura Bazrafshan, Venkatrao Mallipudi and Tim Niggemann. We also gratefully acknowledge Florian Berghammer for his assistance in preparing the FBG instrumentation, and Collins Aerospace, especially Pete Carini and colleagues, for their support with the Aeromini Interrogator. The authors also thank Professor Yavrucuk for his support throughout this project.

Supported by

Bavarian Ministry of Economic Affairs,
Regional Development and Energy

Supported by:

Federal Ministry
for Economic Affairs
and Climate Action

on the basis of a decision
by the German Bundestag

REFERENCES

1. Isom, J. D., Davis, M. W., Cycon, J. P., Rozak, J. N., and Fletcher, J. W., "Flight Test of Technology for Virtual Monitoring of Loads," American Helicopter Society 69th Annual Forum, 2013.

2. CAA Safety Regulation Group, "CAA Paper 2008/05 - HUMS Extension to Rotor Health Monitoring," Technical report, Civil Aviation Authority, 2009.

3. Ganguli, R., Chopra, I., and Haas, D. J., "Helicopter Rotor-System Damage Detection," 2nd International Aeromechanics Specialists' Conference, October 1995.

4. Ganguli, R., Chopra, I., and Haas, D. J., "A Physics-Based Model for Rotor System Health Monitoring," *European Rotorcraft Forum*, September 1996.

5. Ganguli, R., Chopra, I., and Haas, D. J., "Detection of Helicopter Rotor System Simulated Faults using Neural Networks," Structural Dynamics and Materials Conference and Adaptive Structures Forum, April 1996.

6. Ganguli, R., Chopra, I., and Haas, D. J., "Formulation of a Rotor-System Damage Detection Methodology," *Journal of the American Helicopter Society*, Vol. 41, (4), October 1996.

7. Ganguli, R., Chopra, I., and Haas, D. J., *Helicopter Rotor System Health Monitoring using Numerical Simulation and Neural Network*, American Helicopter Society, Virginia Beach VA, May 1997.

8. Ganguli, R., Chopra, I., and Haas, D. J., "Helicopter Rotor System Fault Detection using Physics-Based Model and Neural Networks," *AIAA Journal*, Vol. 36, (6), June 1998.

9. Azzam, H., and Andrew, M., "The use of Math-Dynamic Models to Aid the Development of Integrated Health and Usage Monitoring Systems," *Proceedings of the Institution of Mechanical Engineers, Part G: Journal of Aerospace Engineering*, Vol. 206, (1), 1991, pp. 71–76.

10. Azzam, H., "The Use of Mathematical Models and Artificial Intelligence Techniques to Improve HUMS Prediction Capabilities," *The Royal Aeronautical Society*, 1997.

11. cistia Gallimard, C. D., Nikolajevic, K., Jouve, J., and Beroul, F., "Direct Load Recognition and Damage Estimation using Supervised Learning," Vertical Flight Society's 77th Annual Forum, 2021.

12. cistia Gallimard, C. D., Beroul, F., Denoulet, J., Nikolajevic, K., Pinna, A., Granado, B., and Marsala, C., "Harmonic Decomposition to Estimate Periodic Signals using Machine Learning Algorithms: Application to Helicopter Loads," 2022 International Joint Conference on Neural Networks (IJCNN) —, July 2022. DOI: 10.1109/ijcnn55064.2022.9892736.

13. Favale, M., Davide, P., and Trezzini, A. A., "Prediction of AW609 Rotor Loads by Means of Neural Networks," Vertical Flight Society's 75th Annual Forum, 2019.

14. Graziani, A., Prederi, D., Trezzini, A. A., Masarati, P., and Favale, M., "Prediction of Helicopter Rotor Loads and Fatigue Damage Evaluation with Neural Networks," European Rotorcraft Forum 2022, 2022.

15. Hajek, M., Manner, S., and Suesse, S., "Blade Root Integrated Optical Fiber Bragg Grating Sensors – A Highly Redundant Data Source For Future HUMS," *American Helicopter Society 71st Annual Forum*, 2015.

16. Manner, S., *Validierung eines hybriden Sensornetzwerks im Hubschrauberrotorblatt*, Dissertation, Technische Universität München, München, 2016.

17. Suesse, S., and Hajek, M., "Rotor Blade Displacement and Load Estimation with Fiber-Optical Sensors for a Future Health and Usage Monitoring System," American Helicopter Society 74th Annual Forum, 2018.

18. Pflumm, T., Barth, A., Kondak, K., and Hajek, M., "Auslegung und Konstruktion eines Hauptrotorblattes für ein in extremen Flughöhen operierendes Drehflügel-UAV," Deutscher Luft- und Raumfahrtkongress, Rostock, 2015.

19. Bottasso, L. M., Sala, G., Bettini, P., Tagliabue, P., Corbani, F., Platini, E., Guerra, A. B., and Anelli, A., "Rugged Fiber Optics Monitoring System for Helicopter Rotor Blades," 44th European Rotorcraft Forum, Delft, The Netherlands, 2018.

20. James, S. W., Kissinger, T., Weber, S., Mullaney, K., Chehura, E., Pekmezci, H. H., Barrington, J. H., Staines, S. E., Charrett, T. O. H., Lawson, N. J., Lone, M., Atack, R., and Tatam, R. P., "Fibre-optic measurement of strain and shape on a helicopter rotor blade during a ground run: 1. Measurement of strain," *Smart Materials and Structures*, Vol. 31, (7), June 2022, pp. 075014. DOI: 10.1088/1361-665x/ac736d.

21. Weber, S., Kissinger, T., Chehura, E., Staines, S., Barrington, J., Mullaney, K., Fragonara, L. Z., Petrunin, I., James, S., Lone, M., and Tatam, R., "Application of fibre optic sensing systems to measure rotor blade

structural dynamics," *Mechanical Systems and Signal Processing*, Vol. 158, September 2021, pp. 107758. DOI: 10.1016/j.ymssp.2021.107758.

22. Kissinger, T., Correia, R., Charrett, T. O. H., James, S. W., and Tatam, R. P., "Fiber Segment Interferometry for Dynamic Strain Measurements," *Journal of Lightwave Technology*, Vol. 34, (19), October 2016, pp. 4620–4626. DOI: 10.1109/jlt.2016.2530940.

23. James, S. W., Kissinger, T., Chehura, E., Mullaney, K., Pekmezci, H. H., Barrington, J. H., Staines, S. E., Tatam, R. P., Lone, M., and Weber, S., "Dynamic and Measurement of Strain and Shape on a Rotating and Helicopter Rotor," Proceedings - ettc2020, 2016. DOI: 10.5162/ettc2020/1.5.

24. Kissinger, T., James, S. W., Weber, S., Mullaney, K., Chehura, E., Pekmezci, H. H., Barrington, J. H., Staines, S. E., Charrett, T. O. H., Lawson, N. J., Lone, M., Atack, R., and Tatam, R. P., "Fibre-optic measurement of strain and shape on a helicopter rotor blade during a ground run: 2. Measurement of shape," Vol. 31, June 2022. DOI: 10.1088/1361-665x/ac736c.

25. Berghammer, F., Heuschneider, V., and Hajek, M., "Development and Integration of a Fiber-Optical Sensor System for Rotor Blade State Observation," Proceedings of the Vertical Flight Society 78th Annual Forum, May 2022. DOI: 10.4050/f-0078-2022-17559.

26. Berghammer, F., Sosa, B., Heuschneider, V., Yavrucuk, I., and Hajek, M., "Testing of a Fiber-Optical Sensor System for Rotor Blade HUMS," Proceedings of the Vertical Flight Society 79th Annual Forum, May 2023. DOI: 10.4050/f-0079-2023-18090.

27. Heuschneider, V., Berghammer, F., Pflumm, T., and Hajek, M., "Development and Initial Hover Testing of the Mach Scaled Rotor Test Rig MERIT," 47th European Rotorcraft Forum, United Kingdom, 2021.

28. Pflumm, T., Jochum, A., and Süße, S., "Strain-based Shape Reconstruction and Temperature Compensation for Fiber Bragg-Instrumented Rotor Blades," 50th European Rotorcraft Forum, 2024.

29. Amzallag, C., Gerey, J., Robert, J., and Bahuaud, J., "Standardization of the rainflow counting method for fatigue analysis," *International Journal of Fatigue*, Vol. 16, (4), 1994, pp. 287–293. DOI: https://doi.org/10.1016/0142-1123(94)90343-3.

30. Marsh, G., Wignall, C., Thies, P. R., Barltrop, N., Incecik, A., Venugopal, V., and Johanning, L., "Review and application of Rainflow residue processing techniques for accurate fatigue damage estimation," *International Journal of Fatigue*, Vol. 82, 2016, pp. 757–765. DOI: https://doi.org/10.1016/j.ijfatigue.2015.10.007.